a positive (red to blue) chirp on the driving pulse can result in both a red shift and a spectral narrowing of the harmonic emission peaks[19] (although in that case no dramatic increase in brightness or selectivity was observed). The measured width of the optimized 27th harmonic is 0.24 eV, corresponding to our instrument resolution. Thus, the true peak and spectral enhancements may be even higher. Since the duration of the XUV pulse is probably somewhat shorter than the driving laser pulse, the resulting HHG spectrum corresponds to an XUV pulse much closer to the time-bandwidth limit than before optimization. This result illustrates quite clearly that pulse shaping can alleviate what had been thought to be a fundamental 'trade-off' for use of HHG as a light source—that the use of very short driving pulses, although dramatically increasing the efficiency of HHG, results in a broader spectrum for the individual harmonic peaks.

To explain the unexpected result that very slight changes in laser pulse shape can dramatically enhance and select individual harmonics, we consider the semi-classical rescattering model of HHG[25,26]. From a classical point of view, electrons are ionized and accelerated away from the core during one half-cycle of the laser field, and can be subsequently driven back to the core when the laser field reverses. Some fraction of the ionized electrons can recombine with the parent ion and give off their energy in the form of high harmonics. This process occurs over a few optical cycles of the laser field, resulting in an approximately 5-fs X-ray burst. Particular harmonics are generated by electrons returning to the core with a specific return energy that is related to the exact time within the optical cycles when the electron is initially ionized.

We believe that the adaptive optimization algorithm finds a pulse with the correct phase sequence to ensure that the continuum X-ray emission generated by a particular cycle of the laser pulse reinforces constructively or destructively with different parts of the continuum generated by adjacent cycles. This coherent control can lead to channelling and redirection of energy between different high-order nonlinear interactions.

These findings therefore demonstrate a new type of intra-atomic 'phase matching' between the laser field and the wavefunction of the ionized electron. Preliminary calculations based on phase-only pulse shaping confirm this interpretation. From a quantum point of view, our optimized laser pulse can adjust the quantum phase of the electron wavefunction which returns to the core, to optimize it for a particular harmonic feature. This work may lead to other new methods for control of highly nonlinear systems, as well as improving the utility of the HHG source for application experiments in a broad range of science[27–30]. □

Received 2 March; accepted 15 May 2000.

1. McPherson, A. *et al.* Studies of multiphoton production of vacuum-ultraviolet radiation in the rare gasses. *J. Opt. Soc. Am. B* **4,** 595-601 (1987).
2. Macklin, J. J., Kmetec, J. D. & Gordon, C. L. III High-order harmonic generation using intense femtosecond pulses. *Phys. Rev. Lett.* **70,** 766–769 (1993).
3. L'Huillier, A. & Balcou, P. High-order harmonic generation in rare gases with a 1-ps 1053 nm laser. *Phys. Rev. Lett.* **70,** 774–777 (1993).
4. Chang, Z., Rundquist, A., Wang, H., Murnane, M. M. & Kapteyn, H. C. Generation of coherent X-rays at 2.7 nm using high harmonics. *Phys. Rev. Lett.* **79,** 2967–2970 (1997).
5. Spielmann, C. *et al.* Generation of coherent X-rays in the water window using 5-femtosecond laser pulses. *Science* **278,** 661–664 (1997).
6. Rettenberger, A., Leiderer, P., Probst, M. & Haight, R. Ultrafast electron transport in layered semiconductors studied with femtosecond-laser photoemission. *Phys. Rev. B* **56,** 12092–12095 (1997).
7. Descamps, D. *et al.* Extreme ultraviolet interferometry measurements with high-order harmonics. *Opt. Lett.* **25,** 135–137 (2000).
8. Wefers, M. & Nelson, K. Analysis of programmable ultrashort waveform generation using liquid-crystal spatial light-modulators. *J. Opt. Soc. Am. B* **12,** 1343–1362 (1995).
9. Judson, R. & Rabitz, H. Teaching lasers to control molecules. *Phys. Rev. Lett.* **68,** 1500–1503 (1992).
10. Warren, W., Rabitz, H. & Dahleh, M. Coherent control of quantum dynamics: the dream is alive. *Science* **259,** 1581–1589 (1993).
11. Weinacht, T. C., Ahn, J. & Bucksbaum, P. H. Controlling the shape of a quantum wavefunction. *Nature* **397,** 233–235 (1999).
12. Meshulach, D. & Silberberg, Y. Coherent quantum control of two-photon transitions by a femtosecond laser pulse. *Nature* **396,** 239–242 (1998).
13. Meshulach, D. & Silberberg, Y. Coherent quantum control of multiphoton transitions by shaped ultrashort optical pulses. *Phys. Rev. A* **60,** 1287–1292 (1999).
14. Assion, A. *et al.* Control of chemical reactions by feedback-optimized phase-shaped femtosecond laser pulses. *Science* **282,** 919–922 (1998).
15. Rundquist, A. *et al.* Phase-matched generation of coherent soft X-rays. *Science* **280,** 1412–1415 (1998).
16. Roos, L. *et al.* Controlling phase matching of high-order harmonic generation by manipulating the fundamental field. *Phys. Rev. A* **60,** 5010–5018 (1999).
17. Altucci, C., Bruzzese, R., D'Antuoni, D., de Lisio, C. & Solimeno, S. Harmonic generation in gases by use of Bessel-Gauss laser beams. *J. Opt. Soc. Am. B* **17,** 34–42 (2000).
18. Zhou, J., Peatross, J., Murnane, M. M., Kapteyn, H. C. & Christov, I. P. Enhanced high harmonic generation using 25 femtosecond laser pulses. *Phys. Rev. Lett.* **76,** 752–755 (1996).
19. Chang, Z., Rundquist, A., Wang, H., Kapteyn, H. C. & Murnane, M. M. Temporal phase control of soft-X-Ray harmonic emission. *Phys. Rev. A* **58,** R30–R33 (1998).
20. Salieres, P., Antoine, P., de Bohan, A. & Lewenstein, M. Temporal and spectral tailoring of high-order harmonics. *Phys. Rev. Lett.* **81,** 5544–5547 (1998).
21. Zeek, E. *et al.* Adaptive pulse compression for transform-limited 15fs high-energy pulse generation. *Opt. Lett.* **25,** 587–589 (2000).
22. Zeek, E. *et al.* Pulse compression using deformable mirrors. *Opt. Lett.* **24,** 493–495 (1999).
23. Yelin, D., Meshulach, D. & Silberberg, Y. Adaptive femtosecond pulse compression. *Opt. Lett.* **22,** 1793–1795 (1997).
24. DeLong, K. W., Trebino, R., Hunter, J. & White, W. E. Frequency-resolved optical gating with the use of second-harmonic generation. *J. Opt. Soc. Am. B* **11,** 2206–2215 (1994).
25. Kulander, K. C., Schafer, K. J. & Krause, J. L. in *Super-Intense Laser-Atom Physics* (eds Piraux, B., L'Huillier, A. & Rzazewski, K.) 95–110 (Plenum, New York, 1993).
26. Lewenstein, M., Balcou, P., Ivanov, M. Y. & Corkum, P. B. Theory of high-harmonic generation of low-frequency laser fields. *Phys. Rev. A* **49,** 2117–2132 (1993).
27. Ditmire, T. *et al.* Nuclear fusion from explosions of femtosecond laser-heated deuterium clusters. *Nature* **398,** 489–492 (1999).
28. LeBlanc, S. P. *et al.* Temporal characterization of a self-modulated laser wakefield. *Phys. Rev. Lett.* **77,** 5381–5384 (1996).
29. de Boeij, W. P., Pshenichnikov, M. S. & Wiersma, D. A. Ultrafast solvation dynamics explored by femtosecond photon echo spectroscopies. *Ann. Rev. Phys. Chem.* **49,** 99–123 (1998).
30. Schoenlein, R. W. *et al.* Femtosecond X-ray pulses at 0.4 angstrom generated by 90 degrees Thomson scattering: A tool for probing the structural dynamics of materials. *Science* **274,** 236–238 (1996).

Acknowledgements

We gratefully acknowledge support for this work from the Department of Energy and the National Science Foundation.

Correspondence and requests for materials should be addressed to H. C. K. (e-mail: kapteyn@jila.colorado.edu).

Configurational entropy and diffusivity of supercooled water

Antonio Scala*†, Francis W. Starr*†, Emilia La Nave*, Francesco Sciortino‡ & H. Eugene Stanley*

** Center for Polymer Studies, Center for Computational Science, and Department of Physics, Boston University, Boston, Massachusetts 02215, USA*
‡ Dipartimento di Fisica e Istituto Nazionale per la Fisica della Materia, Universitá di Roma La Sapienza, P.le Aldo Moro 2, I-00185, Roma, Italy

As a liquid approaches the glass transition, its properties are dominated by local potential minima[1,2] in its energy landscape. The liquid experiences localized vibrations in the basins of attraction surrounding the minima, and rearranges via relatively infrequent inter-basin jumps[3]. As a result, the liquid dynamics at low temperature are related to the system's exploration of its own configuration space. The 'thermodynamic approach' to the glass transition considers the reduction in configuration space[4–8] explored as the system cools, and predicts that the configurational entropy[5,9,10] (a measure of the number of local potential energy minima sampled by the liquid) is related to the diffusion constant. Here we report a stringent test of the thermodynamic approach for liquid water (a convenient system to study because of an anomalous pressure dependence in the diffusion constant). We

† Present addresses: Polymers Division and Center for Theoretical and Computational Materials Science, National Institute of Standards and Technology, Gaithersburg, Maryland 20899, USA (F.W.S.); Dipartmento di Fisica e Istituto Nazionale per la Fisica della Materia, Università di Roma La Sapienza, P. le Aldo Moro 2, I-00185, Roma, Italy (A.S.)

calculate the configurational entropy at points spanning a large region of the temperature–density plane, using a model[11] that reproduces the dynamical anomalies of liquid water. We find that the thermodynamic approach can be used to understand the characteristic dynamic anomalies, and that the diffusive dynamics are governed by the configurational entropy. Our results indicate that the thermodynamic approach might be extended to predict the dynamical behaviour of supercooled liquids in general.

One of the most studied models of molecular liquids is the extended simple point charge (SPC/E) potential, designed to model the behaviour of water[11]. The dynamic properties of this model have been studied in detail in the weakly supercooled regime where the diffusion constant decreases by three or four orders of magnitude compared to its normal liquid value ($\sim 10^{-5}\,\mathrm{cm^2\,s^{-1}}$). In this temperature range the SPC/E dynamics have been shown to be consistent[12,13] with the predictions of the mode-coupling theory (MCT)[14,15], and the locus of critical MCT temperatures $T_{MCT}(\rho)$ is also known[13]. The SPC/E potential is of particular interest for testing theories of the supercooled-liquid dynamics because, as observed experimentally for water, the diffusion constant D has a maximum as a function of the pressure P—or of the density ρ—along isotherms, and this maximum becomes more pronounced upon cooling[16].

Here we calculate the SPC/E liquid entropy S, the vibrational entropy S_{vib} of the liquid constrained in one typical basin of the potential energy landscape, and the configurational entropy S_{conf} defined by $S_{conf} \equiv S - S_{vib}$, for state points covering a large region of the (T, ρ) phase diagram. Figure 1 shows the calculated entropies for one particular density. Figure 2a–c shows S, S_{vib} and S_{conf} as functions of ρ for several isotherms. Figure 2d shows the behaviour of D along the same isotherms. Both S_{conf} and D show maxima which become more pronounced with decreasing temperature. Figure 2c and d demonstrates a remarkable correlation between the qualitative behaviours of S_{conf} and D.

Figure 2 also shows that at all temperatures, both D and S_{conf} have maxima at $\rho \approx 1.15\,\mathrm{g\,cm^{-3}}$. The presence of a maximum in S_{conf} at $\rho \approx 1.15\,\mathrm{g\,cm^{-3}}$ is possibly explained by two density-dependent (and nearly temperature-independent) mechanisms balancing. Increasing density in water from the 'ideal' tetrahedral density (for ice, about $0.92\,\mathrm{g\,cm^{-3}}$) leads to the progressive destruction of the hydrogen-bond network. Hence the number of potential energy minima increases (and therefore so does S_{conf}, which is a measure of the number of local landscape minima), as there are more configurations corresponding to a disordered tetrahedral network. At large enough density, core repulsion dominates the liquid properties, and we indeed find that increasing density decreases S_{conf} (as fewer configurations are possible when the system becomes more densely packed).

The close connection between S_{conf} and D shown in Fig. 2 occurs in the same region of the (T, ρ) plane where the dynamics of SPC/E water can be rather well described by MCT[12,13]. Hence MCT appears to capture the reduction of the mobility due to entropic effects.

The phase diagram of liquid water is characterized by the well-known isobaric density maxima line as well as a line of isothermal D maxima. The density maximum line coincides, from the Maxwell relation, $(\partial V/\partial T)_P = -(\partial S/\partial P)_T$, to a line of S extrema. The lines of maximum S and maximum D in real water (Fig. 3a) and in SPC/E simulated water (Fig. 3b), do not coincide. The hypothesis that S_{conf}—not S—is the relevant quantity controlling the dynamics in supercooled states can be tested by comparing the line of isothermal S_{conf} maxima with the line of D maxima. Figure 3b shows that the lines of maxima for S_{conf} and D coincide within calculation uncertainties.

While the thermodynamic approach does not provide a quantitative prediction for D, our calculations allow us to test the functional form relating D and S_{conf} proposed by Adam and Gibbs[5]. In the range of D values that we have probed (Fig. 3c), we find agreement with the linear relation between $\log D$ and $(TS_{conf})^{-1}$ proposed theoretically[5] and verified experimentally in a smaller D range[17].

Our results for S_{conf} permit us to determine the locus of $T_K(\rho)$, which is calculated as the temperature[18] where $S_{conf} \to 0$. Note that Kauzmann defined T_K to be the temperature at which the liquid entropy becomes equal to the crystalline entropy along an isobaric path. Kauzmann's definition coincides with the definition used here if the crystal vibrational entropy is a good approximation to the basin vibrational entropy. Our definition of $T_K(\rho)$ is related to

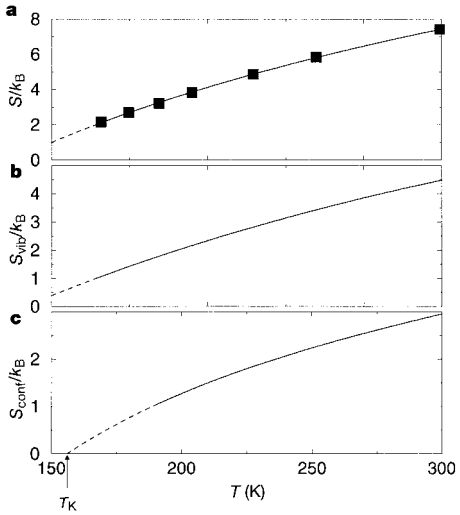

Figure 1 Calculated values of the total vibrational and configurational entropy for one particular isochore, $\rho = 1.0\,\mathrm{g\,cm^{-3}}$. **a**, S; **b**, S_{vib}; **c**, S_{conf}. The arrow indicates the Kauzmann temperature T_K where $S_{conf} \to 0$.

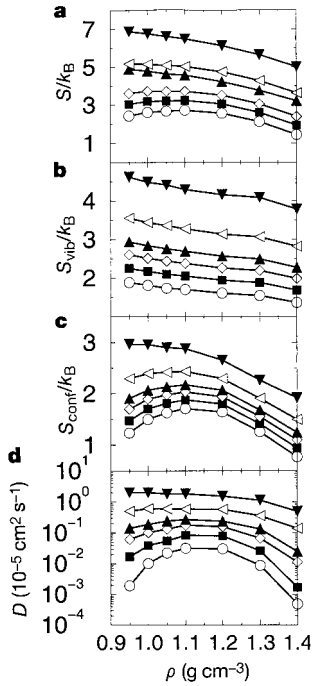

Figure 2 Density dependence of four quantities. **a**, S; **b**, S_{vib}; **c**, S_{conf}; and **d**, D (data from ref. 13), shown along six constant-temperature paths; top to bottom $T = 300$, $T = 260\,\mathrm{K}$, $T = 240\,\mathrm{K}$, $T = 230\,\mathrm{K}$, $T = 220\,\mathrm{K}$, $T = 210\,\mathrm{K}$. We note the close correspondence of densities where the maxima of S_{conf} and D occur.

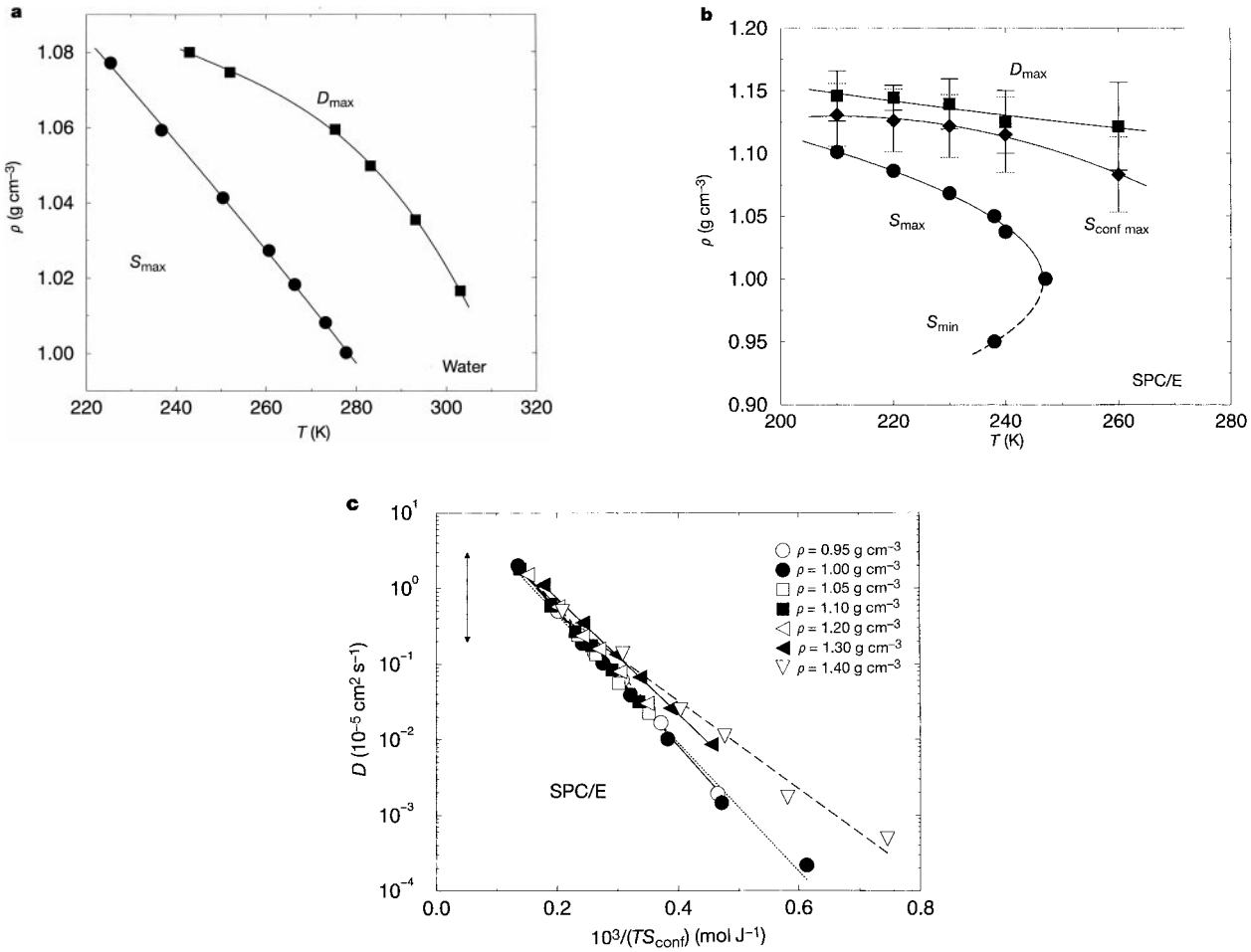

Figure 3 Lines of entropy and diffusion constant extrema, comparing experiments and the present simulations. **a**, Lines of entropy maxima and diffusion constant maxima taken from experimental data on water[16]. **b**, Lines of entropy extrema, configurational entropy maxima, and diffusion constant maxima D for the SPC/E model. Note that the line of entropy maxima does not coincide with the line of diffusion constant maxima. **c**, Semi-log plot of the diffusion constant D versus $(TS_{conf})^{-1}$ for six isochores. The double arrow denotes the range of D values where the relationship log D versus $(TS_{conf})^{-1}$ has been experimentally tested in bulk water[17]. The lines are provided as a guide to the eye.

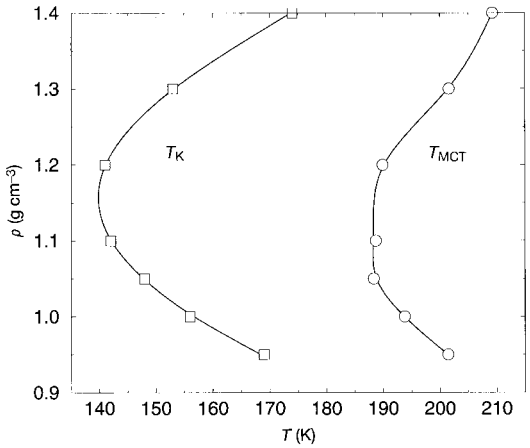

Figure 4 The locus of the mode-coupling theory transition temperature T_{MCT} (ref. 13) and the locus of the Kauzmann temperature T_K. The locus $T_K(\rho)$ is estimated by performing an extrapolation of the (T, ρ) dependence of the configurational entropy. In the context of estimating T_K from the analysis of experimental or numerical data, no distinction can be made between a scenario where S_{conf} indeed goes to zero at T_K (with a clear break in the first T derivative) and a scenario where the extrapolated S_{conf} has a dramatic change in slope and approaches zero only at a much lower T. A slower change in S_{conf} is expected to be accompanied by a slower decrease of D, related to a possible fragile-to-strong transition in water[27–29], a topic of current debate.

the original definition of the Kauzmann temperature because at $T_K(\rho)$, the liquid S_{conf} reaches the crystalline S_{conf}, and thus at $T_K(\rho)$ the number of basins populated in thermal equilibrium is non-extensive. To estimate the difference in the two definitions, we also calculate the purely vibrational ice I_h crystal entropy, and we find that the value for $T_K(\rho)$ is roughly 5 K lower than the one shown in Fig. 4. The locus $T_K(P)$ can be estimated from knowledge of $T_K(\rho)$ and from the equation of state using the implicit relation for the pressure, $P = P(\rho, T_K(\rho))$.

The region $T < T_{MCT}$ defines the region where basin changes require a basin-hopping mechanism[19]. The ratio T_{MCT}/T_K is one measure of the fragility of a liquid[20], and $T_{MCT}/T_K \rightarrow 1$ is expected for an ideal fragile liquid. Figure 4 shows both T_K and T_{MCT}; we see that $T_{MCT}/T_K \approx 1.20$–1.35, indicating that the liquid modelled by the SPC/E potential is fragile in the region of temperatures and densities studied here.

Finally, we note that our approach provides us with an estimate of the free energy which can be extrapolated to low temperature to search for the hypothesized liquid–liquid critical temperature[21,22]. We find that, for the SPC/E potential, the critical point lies below the locus of $T_K(\rho)$ and hence cannot be accessed in equilibrium. □

Methods

Evaluation of $S(T, \rho)$

We first calculate S for a reference point ($T = 1{,}000$ K and $\rho = 1.0\,\mathrm{g\,cm^{-3}}$), and then calculate the entropy as a function of (T, ρ) via thermodynamic integration using the state

points simulated in ref. 13, and new simulations extending to higher temperatures. Specifically, we integrate the relationship $dS = dE/T + PdV/T$ along both constant T and constant V paths. To evaluate S ($T = 1{,}000$ K, $\rho = 1.00\,g\,cm^{-3}$), we perform thermodynamic integration along the $T = 1{,}000$ K isotherm starting from the known analytic value for an ideal gas of rigid triatomic molecules in the infinite volume limit. We verify the reliability of our results for S by checking that $\oint dS = 0$ along several closed P–V cycles. It is convenient to find a functional form to fit the data for $S(T)$. Recently it has been proposed theoretically[23] that—in classical fluids—the temperature dependence of the potential energy at constant volume follows a $T^{3/5}$ law on cooling, contributing an entropy variation that follows a $T^{-2/5}$ law. This temperature dependence has been verified in several atomic system, such as Lennard–Jones, soft spheres, and charged systems in the limit of large densities or low T (ref. 23). We find that temperature dependence is numerically obeyed in our molecular system for $200 < T < 300$, and we use it to generate an analytic expansion for the free energy and the solid line in Fig. 1a.

Calculation of S_{vib}

We use the technique presented in refs 24 and 25 to study the properties of the basins visited by the liquid at equilibrium. For each (T, ρ) we use the conjugate gradient algorithm[25] to calculate—for two independent systems and for 100 configurations—the corresponding local minima, called inherent structures[2]. The configurations we use span a time of at least 25 times the α-relaxation time of the density–density correlation function. We estimate S_{vib} by adding anharmonic corrections to the harmonic contribution $S_{harm} = k_B\Sigma_{i=1}^{6N-3}[\ln(k_BT\hbar\omega_i) - 1]$, where ω_i are the normal-mode frequencies of the inherent structure determined from the Hessian matrix[19]. Here k_B is Boltzmann's constant, N is the number of molecules and $\hbar$ is Planck's constant. The harmonic approximation for a binary Lennard–Jones mixture is a valid estimate of S_{vib} for temperatures around T_{MCT} (refs 25, 26). However, in the case of the SPC/E potential, we find that there are significant anharmonicities in the basins. This can be seen from the fact that, if the system were purely harmonic, the energy E should equal E_{basin}, the energy of a minimum, plus the contribution $E_{harm} = (6N - 3)k_BT/2$ of the harmonic solid approximation. In contrast with the binary mixture Lennard–Jones case[25,26], we find the vibrational contribution $E_{vib} \equiv E - E_{basin}$ to be roughly 10% larger than the harmonic approximation, even at the lowest temperatures studied.

We estimate therefore the anharmonic contributions to S_{vib} by heating inherent structures at constant volume and measuring the deviation of E_{vib} from the harmonic approximation. For each collection of basins corresponding to a particular (T, ρ) state point, we calculate E_{vib} in the range $T = 0$–200 K and fit our results using the approximation $E_{vib} = E_{harm} + aT^2 + bT^3$ with a, b used as fitting parameters. By integrating the relation $dS_{vib} = dE_{vib}/T$, we find $S_{vib} = S_{harm} + 2aT + \frac{3}{2}bT^2$. We have checked that system remains confined in the same basin up to $T \approx 200$ K when heating the inherent structure from $T = 0$ K on the time scale of 200 ps. We have evaluated this anharmonic contribution from the inherent structures of the simulations at $T = 210$ K. However, using the inherent structures generated from higher temperature configurations does not affect our results.

Received 31 January; accepted 5 May 2000.

1. Sastry, S., Debenedetti, P. G. & Stillinger, F. H. Signatures of distinct dynamical regimes in the energy landscape of a glass-forming liquid. *Nature* **393,** 554–557 (1998).
2. Stillinger, F. H. A topographic view of supercooled liquids and glass formation. *Science* **267,** 1935–1939 (1995).
3. Goldstein, M. Viscous liquids and the glass transition: A potential energy barrier picture. *J. Chem. Phys.* **51,** 3728–3739 (1969).
4. Kauzmann, A. W. The nature of the glassy state and the behavior of liquids at low temperatures. *Chem. Rev.* **43,** 219–256 (1948).
5. Adams, G. & Gibbs, J. H. On the temperature dependence of cooperative relaxation properties in glass-forming liquids. *J. Chem. Phys.* **43,** 139–146 (1958).
6. Speedy, R. J. Relations between a liquid and its glasses. *J. Phys. Chem. B* **103,** 4060–4065 (1999).
7. Mézard, M. & Parisi, G. Thermodynamics of glasses: A first principles computation. *J. Phys. Cond. Matter* **11** A157–A165 (1999).
8. Wolfgardt, M., Baschnagel, J., Paul, W. & Binder, K. Entropy of glassy polymer melts: Comparison between Gibbs–DiMarzio theory and simulation. *Phys. Rev. E* **54,** 1535–1543 (1996).
9. Shulz, M. Energy landscape, minimum points, and non-Arrhenius behavior of super-cooled liquids. *Phys. Rev. B* **57,** 11319–11333 (1998).
10. Debenedetti, P. G. *Metastable liquids* (Princeton Univ. Press, Princeton, 1997).
11. Berendsen, H. J. C., Grigera, J. R. & Stroatsma, T. P. The missing term in effective pair potentials. *J. Phys. Chem.* **91,** 6269–6271 (1987).
12. Fabbian, L. *et al.* Molecular mode-coupling theory for supercooled liquids: application to water. *Phys. Rev. E* **60,** 5768–5777 (1999).
13. Starr, F. W., Sciortino, F. & Stanley, H. E. Dynamics of simulates water under pressure. *Phys. Rev. E* **60,** 6757–6768 (1999).
14. Götze, W. & Sjögren, L. Relaxation processes in supercooled liquids. *Rep. Prog. Phys.* **55,** 241–376 (1992).
15. Kob, W. Computer simulations of supercooled liquids and glasses. *J. Phys. Condens. Mat.* **11,** R85–R115 (1999).
16. Prielmeier, F. X., Lang, E. W., Speedy, R. J. & Lüdemann, H.-D. Diffusion in super-cooled water to 300 MPa. *Phys. Rev. Lett.* **59,** 1128–1131 (1987).
17. Angell, C. A., Finch, E. D., Woolf, L. A. & Bach, P. Spin-echo diffusion coefficients of water to 2380 bar and −20 °C. *J. Chem. Phys.* **65,** 3063–3066 (1976).
18. Stillinger, F. H. Supercooled liquids, glass transitions, and the Kauzmann paradox. *J. Chem. Phys.* **88,** 7818–7825 (1988).
19. La Nave, E., Scala, A., Starr, F. W., Sciortino, F. & Stanley, H. E. Instantaneous normal mode analysis of supercooled water. *Phys. Rev. Lett.* **84,** 4605–4608 (2000).
20. Angell, C. A. Formation of glasses from liquids and biopolymers. *Science* **267,** 1924–1935 (1995).
21. Poole, P. H., Sciortino, F., Essmann, U. & Stanley, H. E. Phase behaviour of metastable water. *Nature* **360,** 324–328 (1992).
22. Mishima, O. The liquid–liquid critical point in heavy water. *Phys. Rev. Lett.* **85,** 334–337 (2000).
23. Rosenfeld, Y. & Tarazona, P. Density functional theory and the asymptotic high density expansion of the free energy of classical solids and fluids. *Mol. Phys.* **95,** 141–150 (1998).
24. Coluzzi, B., Verrochio, P. & Parisi, G. Thermodynamical liquid-glass transition in a Lennard-Jones binary mixture. *Phys. Rev. Lett.* **84,** 306–309 (2000).
25. Sciortino, F., Kob, W. & Tartaglia, P. Inherent structure entropy of supercooled liquids. *Phys. Rev. Lett.* **83,** 3214–3217 (1999).
26. Press, W. H., Flannery, B. P., Teukolsky, A. A. & Vetterling, W. T. *Numerical Recipes: The Art of Scientific Computing* (Cambridge Univ. Press, Cambridge, 1986).
27. Ito, K., Moynihan, C. T. & Angell, C. A. Thermodynamic determination of fragility in liquids and a fragile-to-strong liquid transition in water. *Nature* **398,** 492–495 (1999).
28. Smith, R. S. & Kay, B. D. The existence of supercooled liquid water at 150 K. *Nature* **398,** 788–791 (1999).
29. Bergman, R. & Swenson, J. Dynamics of supercooled water in confined geometry. *Nature* **403,** 283–286 (2000).

Acknowledgements

We thank C. A. Angell, S. Sastry and R. J. Speedy for helpful discussions, and the NSF for support. F.S. acknowledges partial support from the Ministero Universitá Ricerca Scientifica e Tecnologica (MURST), Progetto Ricerca Interesse Nazionale (PRIN 98) and the Istituto Nazionale Fisica della Materia-Progetto di Ricerca Avanzata (HOPPING) (INFM-PRA-HOP).

Correspondence and requests for materials should be addressed to A.S. (e-mail: scala@phys.uniroma1.it).

Electronic connection to the interior of a mesoporous insulator with nanowires of crystalline RuO_2

Joseph V. Ryan, Alan D. Berry, Michele L. Anderson, Jeffrey W. Long, Rhonda M. Stroud, Veronica M. Cepak, Valerie M. Browning, Debra R. Rolison & Celia I. Merzbacher

Naval Research Laboratory, 4555 Overlook Avenue, SW, Washington DC, 20375, USA

Highly porous materials such as mesoporous oxides are of technological interest[1] for catalytic, sensing and remediation applications: the mesopores (of size 2–50 nm) permit ingress by molecules and guests that are physically excluded from microporous materials. Connecting the interior of porous materials with a nanoscale or 'molecular' wire would allow the direct electronic control (and monitoring) of chemical reactions and the creation of nanostructures for high-density electronic materials[2]. The challenge is to create an electronic pathway (that is, a wire) within a mesoporous platform without greatly occluding its free volume and reactive surface area[3]. Here we report the synthesis of an electronically conductive mesoporous composite—by the cryogenic decomposition of RuO_4—on the nanoscale network of a partially densified silica aerogel. The composite consists of a three-dimensional web of interconnected (~4-nm in diameter) crystallites of RuO_2, supported conformally on the nanoscopic silica network. The resulting monolithic (RuO_2‖SiO_2) composite retains the free volume of the aerogel and exhibits pure electronic conductivity. In addition to acting as a wired mesoporous platform, the RuO_2-wired silica aerogel behaves as a porous catalytic electrode for the oxidation of chloride to molecular chlorine.

The metallic electronic conductivity of anhydrous RuO_2 (single-crystal conductivity, σ, $\sim 2\times10^4$ S cm^{-1} at 25°C), along with its excellent chemical and thermal stability[4–7], makes this material feasible as a durable nanowire in the presence of water and oxygen,